Journal of Materials Chemistry

Cite this: J. Mater. Chem., 2011, 21, 8566

www.rsc.org/materials

PAPER

Stabilization of Mn(IV) in nanostructured zinc manganese oxide and their facile transformation from nanospheres to nanorods†

Menaka,[a] S. L. Samal,[a] K. V. Ramanujachary,[b] S. E. Lofland,[c] Govind[d] and A. K. Ganguli*[a]

Received 27th January 2011, Accepted 22nd March 2011
DOI: 10.1039/c1jm10425j

Nanostructured ternary manganese(IV) oxides are of importance as electrode materials. A low-temperature, precursor mediated route has been designed to obtain ternary oxides containing Mn(IV) and Zn(II) at ambient pressure. The defect spinel, $Zn_{0.83}(Mn_{1.42}Zn_{0.34})O_4$ was obtained by annealing at optimal conditions after the thermal decomposition of oxalates of zinc and manganese co-precipitated at room temperature. This is the first report of a low temperature (250 °C) and normal atmospheric pressure synthesis of a ternary zinc manganese oxide containing purely tetravalent manganese. Rietveld refinement indicates zinc occupancy in both tetrahedral and octahedral sites with the refined composition of $(Zn_{0.83})_{tet}(Mn_{1.42}Zn_{0.34})_{oct}O_4$. Also, we show for the first time that refluxing with acetic acid transforms the oxide nanospheres (5–20 nm) to nanorods with diameter of 10–15 nm and length varying from 60 to 150 nm. The stoichiometry of Zn and Mn, as well as the oxidation state of manganese has been confirmed by SEM-EDX, PXRD, AAS, XPS and magnetic studies. $Zn_{0.83}(Mn_{1.42}Zn_{0.34})O_4$ is antiferromagnetic with a Néel temperature of ~5–10 K. The rods of 10 nm diameter (aspect ratio = 6) show higher susceptibility values (5 fold enhancement) compared to spherical nanoparticles. This low temperature route can be extended for the design of other material phases.

Introduction

Stabilization of unusual oxidation states has been of great interest and a challenge to inorganic chemists, as many of these compounds are expected to show novel properties. Oxides containing tetravalent manganese are of importance in batteries and super-capacitors as electrodes and as catalysts for the degradation of organic compounds. Tetravalent manganese compounds such as MnO_2 and $AMnO_3$ have been previously reported while the spinels of Mn(IV) are rare. $AMnO_3$ (A = Ca, Ba, Sr, Ni, Co, Zn and Mg) compounds containing Mn(IV) ions normally crystallize in either the ilmenite (A = Ni, Co, Zn and Mg) or the perovskite structure (A = Ca, Ba and Sr).[1] However, almost all the above Mn(IV) compounds have been synthesized at high pressure (sometimes exceptionally high, *e.g.* 3000 atm for $MgMnO_3$). There is no report so far of the synthesis of any Mn (IV) based **ternary** oxides at ambient conditions and low temperature (less than 300 °C), though the binary Mn(IV) oxide (MnO_2) has been synthesized by low temperature routes at ambient pressure.[2] In the Zn–Mn–O ternary system, five phases ($ZnMn_2O_4$, $ZnMnO_3$, $Zn_2Mn_3O_8$, $ZnMn_3O_7$ and Zn_2MnO_4) have been previously reported.[3–11] Out of these phases, one having the formula of $ZnMn_2O_4$ and another purported to have the formula *$ZnMnO_3$* (later shown to be a cubic defect spinel of AB_2O_4 type structure) have been investigated. Blasco *et al.* show that the reported cubic $ZnMnO_3$ is a spinel of type $Zn_xMn_{3-x}O_4$.[11] $Zn_xMn_{3-x}O_4$ ($1 \leq x \leq 2$) crystallizes in two different phases, one having a tetragonal structure (Fig. 1a) with space group $I4_1/amd$, and another having a cubic structure with a $Fd\bar{3}m$ space group (Fig. 1b). The two crystal structures in $Zn_xMn_{3-x}O_4$ have a different average **oxidation state of manganese** (Fig. 1a–b). The tetragonal $Zn_xMn_{3-x}O_4$ (space group $I4_1/amd$) has manganese completely in a + 3 oxidation state, which is quite stable and has been isolated as a pure phase.[7,8] However, the cubic spinel phase found in $Zn_xMn_{3-x}O_4$ has been observed as an impurity phase along with zinc oxide and tetragonal $ZnMn_2O_4$.[9–12] Earlier reports of the cubic spinel phase shows the presence of mixed valent manganese (+3 and +4).[13–16] Solid solutions of tetragonal $Zn_xMn_{3-x}O_4$ ($0.5 \leq x \leq 1.5$) have been synthesized by the citrate route.[11,16] The pure cubic spinel phase of $Zn_xMn_{3-x}O_4$ (space group $Fd\bar{3}m$) forms only in the temperature range of 400–800 °C.[17–19] At higher temperatures the

[a]*Department of Chemistry, Indian Institute of Technology, Hauz Khas, New Delhi, 110016, India. E-mail: ashok@chemistry.iitd.ernet.in; Fax: +91-11-26854715; Tel: +91-11-26591511*
[b]*Department of Chemistry and Biochemistry, Rowan University, Glasboro, NJ, 08028, USA*
[c]*Department of Physics, Rowan University, Glasboro, NJ, 08028, USA*
[d]*Physics of Energy Harvesting, National Physical Laboratory (CSIR), New Delhi, 110012, India*
† Electronic supplementary information (ESI) available: Figures S1 to S5. See DOI: 10.1039/c1jm10425j

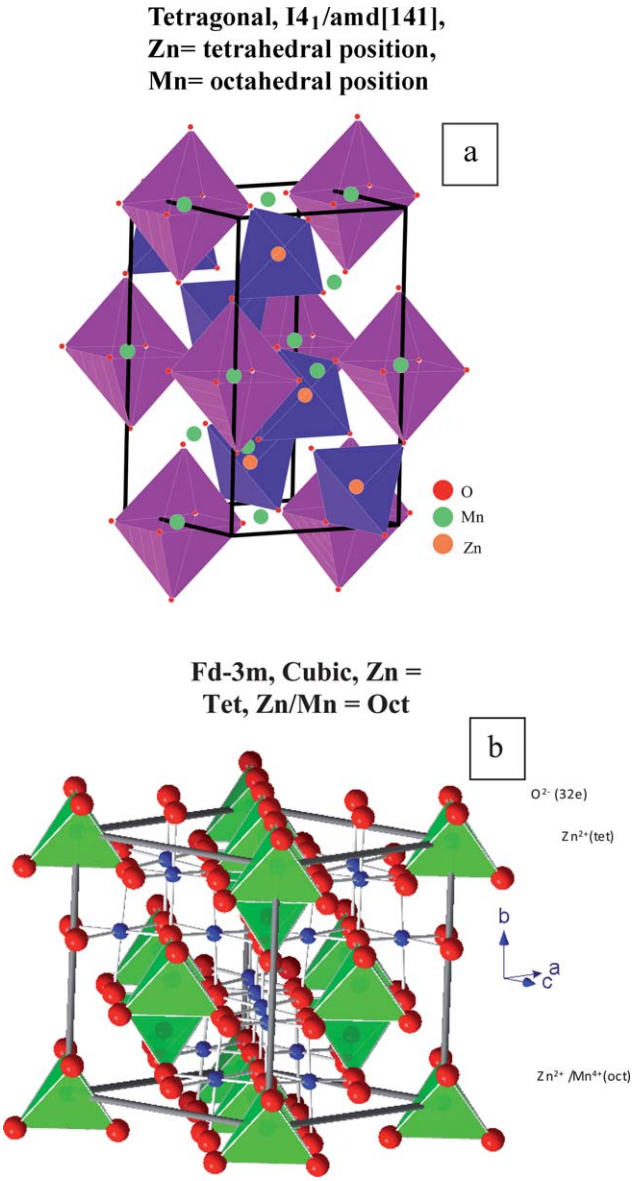

Fig. 1 Structure of tetragonal and cubic spinel AB_2O_4.

metastable cubic spinel is partially transformed to the more stable tetragonal phase. The cubic spinel ($Zn_xMn_{3-x}O_4$) is obtained only when equimolar quantities of zinc and manganese are used in the initial reaction mixture. A higher zinc content in the reaction mixture leads to the formation of ZnO while a lower zinc content leads to the formation of the tetragonal spinel, $ZnMn_2O_4$ (containing only Mn(III) as a minor phase).[16] The cubic spinel $Zn_xMn_{3-x}O_4$ ('so-called cubic $ZnMnO_3$') is synthesized *via* a solid state (800 °C)[20] and sol–gel route (650 °C)[18] at a relatively high temperature compared to the temperature employed by us (250 °C). Our major interest in this research was to stabilize the cubic spinel ($Zn_xMn_{3-x}O_4$) phase with Mn(IV) in order to develop new battery materials. Mn(IV) oxides especially MnO_2 are of interest due to their applications in the battery industry as cathode-active materials. Recently, considerable attention has been directed towards manganese compounds of various morphology and their size dependent optical, magnetic and electronic properties.[14,15] Other than electrode materials, $Zn_xMn_{3-x}O_4$ has been shown to have applications as a catalyst[7] and as a negative thermal coefficient (NTC) material.[8] To the best of our knowledge all previous studies reporting the synthesis and phase diagram of zinc manganese oxides at ambient pressure have been carried out at temperatures ≥400 °C.[11,15–20] The reports on the spinel ($Zn_xMn_{3-x}O_4$) show the stabilization of mixed-valent Mn (III, IV) or only Mn(III) in octahedral sites of the AB_2O_4 type spinel. The assembly of particles and control of their shape is one of the fascinating areas in nanotechnology. Our earlier studies on various manganite systems[7,14] have motivated us to investigate methods to control the nanostructures of ternary oxides. We have developed a simple route for the transformation of nanospheres to nanorods. An important challenge in this study was to maintain the Mn(IV) oxidation state during the transformation of nanosphere to nanorod. The present study discusses the stabilization of the nanostructured (nanospheres and nanorods) cubic spinel phase of $Zn_{0.83}(Mn_{1.42}Zn_{0.34})O_4$, containing purely tetravalent Mn(IV) obtained by a low temperature, precursor-mediated route at ambient pressure. The magnetic studies of these oxides show antiferromagnetic behaviour with a Néel temperature of 5–10 K.

Results and discussion

Structure and compositional analysis

Oxalate precursor of zinc and manganese. The powder X-ray diffraction pattern of the oxalate precursors obtained by the co-precipitation method (at room temperature) shows the formation of a mixture of zinc oxalate dihydrate and manganese oxalate dihydrate (Fig. S1†). The atomic absorption study of the oxalate precursor shows that the ratio of Zn : Mn is 2 : 1. SEM–EDX (Fig. S2†) carried out over a large area (250 μm × 500 μm) of a pelletized sample also shows the ratio of Zn : Mn to be 2 : 1. It may be noted that the loaded composition of the oxalate precursor contains a Zn : Mn ratio of 1 : 21. The marked variation in the loaded and experimentally evaluated composition of oxalate precursor is because of the different rate of precipitation of the zinc oxalate (higher rate) and manganese oxalate.[22] Thermogravimetric analysis of the oxalate precursor carried out in flowing nitrogen shows two regions of weight loss, the first at 150 °C corresponds to loss of two water molecules and the second at 400 °C corresponds to loss of carbon dioxide and carbon monoxide (Fig. S3†). It may be noted that synthesis of Zn–Mn–O compounds and earlier studies on the phase diagram[21,22] have been carried out above 400 °C. There is no report on the synthesis of Zn–Mn–O phases at temperatures below 400 °C and at ambient pressure. Although, the hydrothermal route for the synthesis of the Mn(III) spinel $ZnMn_2O_4$ is carried out at 120 °C.[23]

Zinc manganese oxide. The oxalate precursor was separately heated at 250 °C, 450 °C and 600 °C and the product was refluxed in acetic acid (0.1 M) to remove the excess zinc oxide. The PXRD pattern of the product obtained at 250 °C and 450 °C was similar to the reported 'cubic $ZnMnO_3$' phase[13,20] (JCPDS card no. 191461) (Fig. 2a–b). However, the PXRD pattern of the product obtained at 600 °C shows the presence of the above mentioned

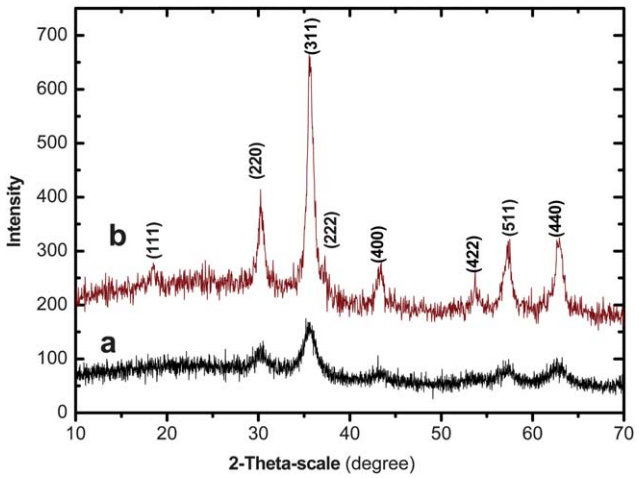

Fig. 2 PXRD pattern of the calcined product obtained at (a) 250 °C and (b) 450 °C showing the presence of spinel zinc manganese oxide.

phase along with ZnO (8%) as an impurity (this will be discussed later). The powder X-ray diffraction pattern of the product obtained at 250 °C shows that the product was poorly crystalline (Fig. 2a). As, we raised the temperature of calcination, the crystallinity of the product improved gradually (Fig. 2b). The X-ray diffraction pattern of the oxide obtained at 600 °C is very close to the **so called $ZnMnO_3$**[20] as discussed earlier. However, a careful study (with the slow scan data) shows the presence of minor impurity of ZnO (8%) (Fig. 3a). Chemical analysis (AAS) and EDX studies of all the products (obtained at 250 °C, 450 °C and 600 °C) shows a Zn : Mn ratio of 2 : 1 which is close to the Zn : Mn ratio in the oxalate precursor discussed earlier. It seems that the excess zinc oxalate converted to amorphous ZnO which can be detected by the AAS analysis (as AAS requires dissolution of the products). To remove ZnO, the products (all as-obtained products at 250 °C, 450 °C and 600 °C) were refluxed at 120 °C for 6 h in acetic acid. There is no change in PXRD pattern of the refluxed product obtained **at 250 °C and 450 °C** and is similar to the PXRD patterns discussed earlier for the oxides before reflux (Fig. 2a–b). **However the product obtained at 600 °C shows the absence of ZnO impurity after refluxing** (Fig. 3b). The AAS and

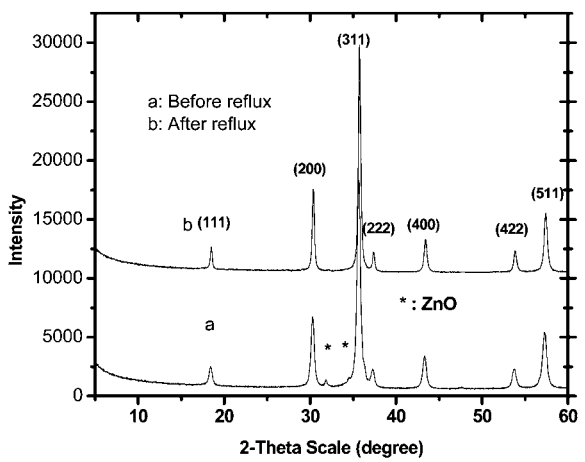

Fig. 3 PXRD pattern of the calcined product obtained (a) 600 °C and (b) refluxed product of 600 °C showing the presence of spinel zinc manganese oxide.

SEM-EDX studies (Fig. S4a-b†) of the refluxed product shows Zn : Mn in the ratio of **1 : 1.21** which confirms the absence of ZnO in the refluxed samples. The structure of the ternary oxide obtained at 450 °C and 600 °C (followed by reflux in acetic acid at 120 °C) could be refined satisfactorily (Rietveld method) with a refined composition of $(Zn_{0.83(2)})_{tet}(Mn_{1.42(1)}Zn_{0.34(1)})_{Oct}O_4$ (Fig. 4a) and $(Zn_{0.83(3)})_{tet}(Mn_{1.42(1)}Zn_{0.34(1)})_{Oct}O_4$ (Fig. 4b) respectively. The *R*-factor and χ^2 values indicate a good quality of refinement (Fig. 4a–b). The relevant crystallographic parameters are included in Table 1a and b. The refined occupancy factors show, 83% of the tetrahedral sites are occupied by Zn while the octahedral sites are occupied partially by Mn (71%) and Zn (17%). It is rare to have Zn occupy octahedral sites ($3d^{10}$ electronic configuration) and it is known to occupy tetrahedral sites in most of its compounds. The occupancy of Zn in an octahedral site for a Zn–Mn–O system has been discussed previously by Blasco *et.al.*[13]

Oxidation state of manganese in zinc manganese oxide

The oxidation state of manganese in the ternary zinc manganese oxide has been investigated using XPS, magnetic and Rietveld refinement studies (Table 1a and b). X-ray photoelectron spectroscopy (XPS) studies of the as obtained products at each stage have been analyzed. The core level spectra of Mn (2p) shows two peaks at binding energies 642.1 eV and 653.8 eV, which correspond to the $2p_{3/2}$ and $2p_{1/2}$ levels respectively, and the peak separation between $2p_{3/2}$ & $2p_{1/2}$ is observed to be 11.70 eV (Fig. 5). To evaluate the oxidation state of the Mn, the FWHM (Full Width Half Maxima) of the Mn $2p_{3/2}$ core level spectra is measured using peak-fit software. The FWHM of the Mn $2p_{3/2}$ peak is found to be 3.33 eV at the binding energy value 642.1 eV (shown as an inset of Fig. 5) which confirms the presence of Mn in the IV oxidation state reported earlier.[28] Further, the magnetic moment, 3.77 μ_B, also suggests the presence of tetravalent manganese.

Size and morphology of zinc manganese oxide. Transmission electron microscopic analysis (TEM) studies of the oxalate precursors show spherical nanoparticles with an average size of 80–100 nm (Fig. S5†). TEM micrographs of the **$Zn_{0.83}(Mn_{1.42}Zn_{0.34})O_4$** obtained by the co-precipitation method at 250 °C and 450 °C shows spherical nanoparticles with sizes of around 5–10 nm and 10–20 nm respectively (Fig. 6a and 7a). The product obtained at 250 °C has the lowest particle size compared to all the previous reports on zinc manganese oxide (lowest reported size was 20–30 nm).[7,25–27] The ability to synthesize materials at low temperatures generally yields fine particles. HRTEM studies of the spinel phases obtained at 250 °C and at 450 °C show the crystalline nature of the nanorods, as shown by the regular lattice fringes (Fig. 6b and 7b). The electron diffraction pattern of **$Zn_{0.83}(Mn_{1.42}Zn_{0.34})O_4$** obtained at 250 °C confirms the cubic structure and the sharp spots indicate the crystallinity of the particles (Fig. 6c). A TEM micrograph of the product obtained after refluxing of the 250 °C, 450 °C and 600 °C heated samples shows the formation of nanorods with aspect ratios 6 (250 °C, dia = 10 nm, length = 60 nm) (Fig. 8a), 10 (450 °C, dia = 15 nm, length = 150 nm) (Fig. 9a) and 10 (diameter 50–60 nm, length 300–500 nm and aspect ratio 6–10)

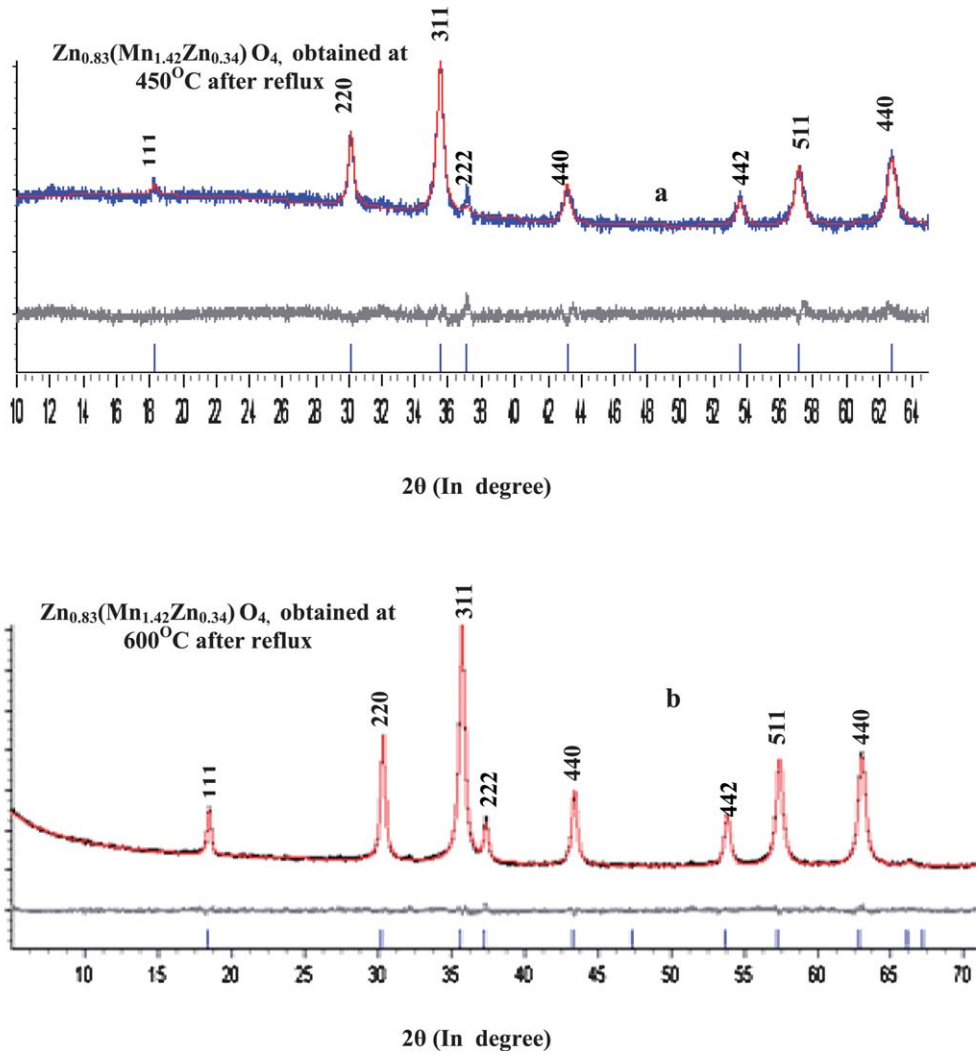

Fig. 4 Rietveld plot of refluxed product obtained at (a) 450 °C and (b) 600 °C by decomposition of oxalate precursors.

Table 1 Refined positional and thermal parameters for $Zn_{0.83}(Mn_{1.42}Zn_{0.34})O_4$ (a) obtained at 450 °C followed by refluxing in acetic acid and (b) obtained at 600 °C followed by refluxing in acetic acid. Relative position along *c* axis (*z*), occupation number (*n*), and the isotropic thermal factor, (U_{iso}). The numbers in parentheses are the estimated standard deviations in the last digit

(a) Space group = $Fd\bar{3}m$, *a*/Å 8.377(2), R_{exp}: 5.77 R_{wp}: 6.78 R_p: 5.29 χ^2: 1.17

	Position				
Atoms	*X*	*Y*	*Z*	U_{iso} (Å^2)	Fractional occupancy
Zn	0	0	0	0.774(1)	0.8301(2)
Mn	0.625	0.625	0.625	1.84(6)	0.710(4)
Zn	0.625	0.625	0.625	1.28 (9)	0.1714(7)
O	0.3850 (5)	0.3850 (5)	0.3850 (5)	1.25 (6)	1

(b) Space group = $Fd\bar{3}m$, *a*/Å: 8.3563(1); R_{exp}: 3.16, R_{wp}: 4.06, $\chi^2 = 1.22$

	Position				
Atoms	*X*	*Y*	*Z*	U_{iso} (Å^2)	Fractional occupancy
Zn	0	0	0	0.49(2)	0.8305(6)
Mn	0.625	0.625	0.625	0.84(1)	0.711(2)
Zn	0.625	0.625	0.625	0.610 (7)	0.178(9)
O	0.3845 (5)	0.3845 (5)	0.3845 (5)	1.025 (3)	1

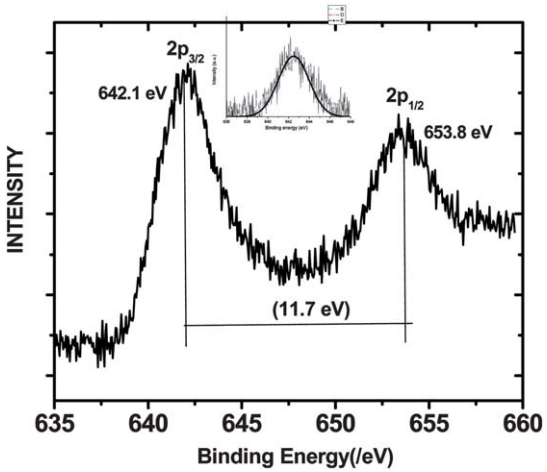

Fig. 5 X-ray photoelectron spectra of product obtained (at 600 °C) after reflux shows the presence of tetravalent manganese, an inset shows the fitted curve for $^2P_{3/2}$ peak.

(Fig. 10a) respectively. It may be noted that the oxide obtained at 250 °C and 450 °C led to nanoparticles of 5–10 nm and 10–20 nm, respectively, and the oxide, $Zn_{0.83}(Mn_{1.42}Zn_{0.34})O_4$, obtained after reflux shows rod-like morphology. The probable reason for such a morphological transition from spherical nanoparticles to nanorods is the templating effect of acetic acid which was used as a refluxing solvent for the removal of ZnO. It is known that adsorbed acetate groups act as a bidentate ligand[29,30] which facilitates the growth of nanorods from the nanoparticles. The growth of zinc oxide nanorods from spherical particles in the presence of acetic acid has been reported previously.[30,31] Extensive studies on metal oxalate nanostructures have shown the formation of nanorods in the presence of carboxylate ions.[32] HRTEM studies of aligned nanorods of the spinel phase **$Zn_{0.83}(Mn_{1.42}Zn_{0.34})O_4$** were obtained after reflux (Fig. 10a). The crystalline nature of the nanorod is shown by the regular lattice fringes (Fig. 9b and 10 b). This is the first report of the synthesis of any spinel in the Zn–Mn–O system at such a low temperature. These nanostructures have the lowest size previously reported for zinc manganese oxide (Note that there are no reports on nanorods of Zn–Mn-oxide while the lowest particle size reported earlier was 25 nm). We believe that on heating the mixture of zinc oxalate and manganese oxalate in air at low temperature (250–450 °C) led to the formation of ZnO and MnO_2 at an intermediate stage and then the reaction subsequently led to the formation of $Zn_{0.83}(Mn_{1.42}Zn_{0.34})O_4$ under optimized conditions. It is known that the decomposition of manganese oxalate in air at 450 °C leads to the formation of Mn_2O_3[24] whereas low temperature decomposition of the manganese precursor (<300 °C) results in the formation of MnO_2, stabilizing Mn in the tetravalent state.[28] When heated at low temperature the oxalate precursor (250– 450 °C) facilitates the formation of higher-valent manganese which further reacts with zinc oxide, formed under the same environment, to form $Zn_{0.83}(Mn_{1.42}Zn_{0.34})O_4$ with tetravalent manganese.

Magnetic properties of zinc manganese oxide. The magnetic properties of the spinel $Zn_{0.83}(Mn_{1.42}Zn_{0.34})O_4$ shows an antiferromagnetic behavior and the magnetic moment, Néel

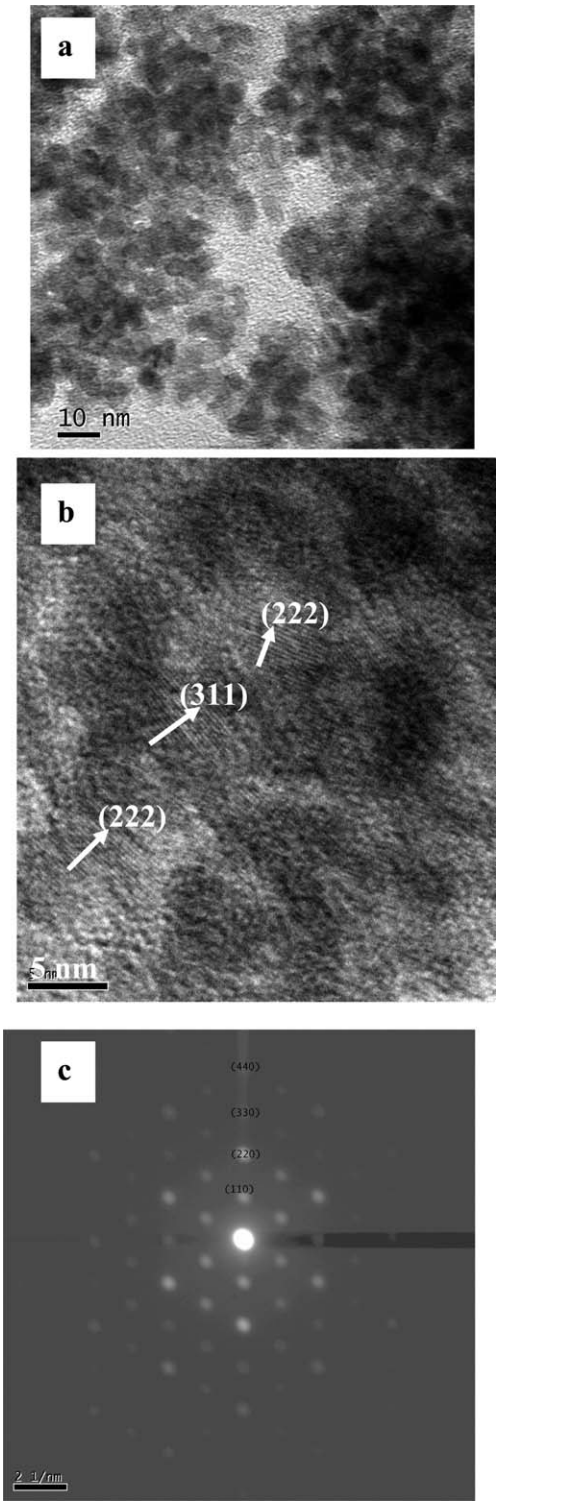

Fig. 6 $Zn_{0.83}(Mn_{1.42}Zn_{0.34})O_4$ nanoparticles synthesized by a co-precipitation method at 250 °C in air; (a) TEM (b) HRTEM and c) electron diffraction pattern.

temperature and θ values are tabulated in Table. 2 (Fig. 11a–b). The effective magnetic moments were calculated using the formula "$Zn_{0.83}(Mn_{1.42}Zn_{0.34})O_4$" in which we have considered ZnO as a non-magnetic impurity. The effective magnetic moment

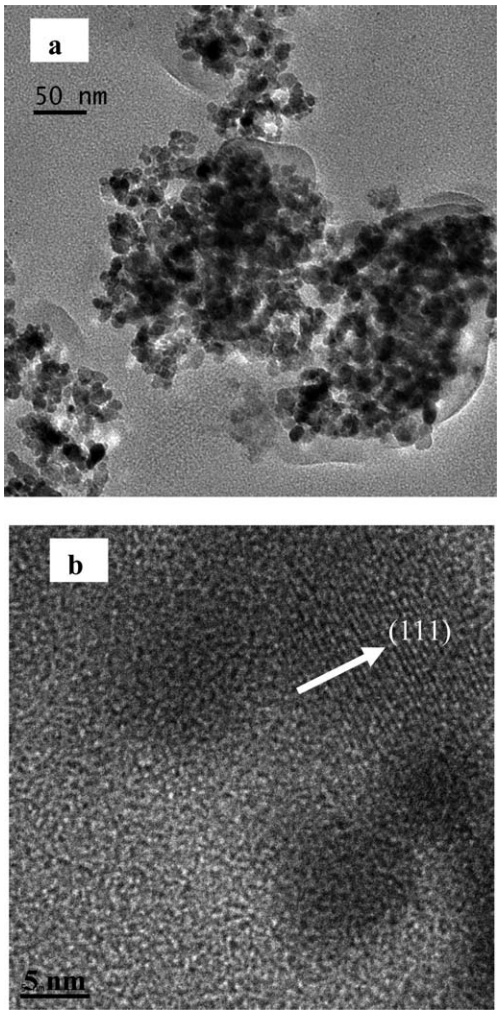

Fig. 7 $Zn_{0.83}(Mn_{1.42}Zn_{0.34})O_4$ nanoparticles synthesized by a co-precipitation method at 450 °C in air; (a) TEM and (b) HRTEM.

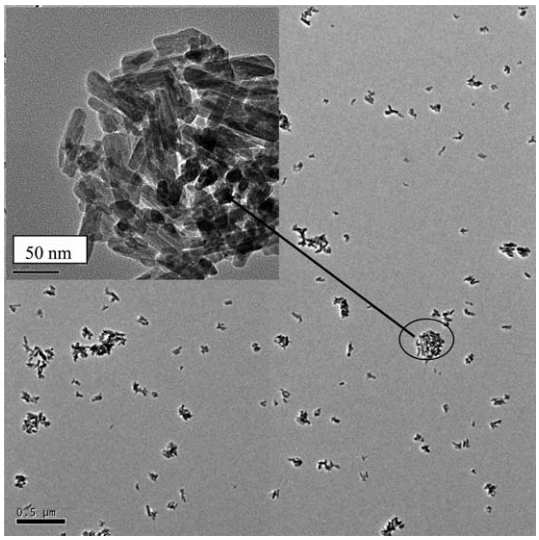

Fig. 8 Transmission electron micrograph of $Zn_{0.83}(Mn_{1.42}Zn_{0.34})O_4$ nanorods synthesized by thermal decomposition at 250 °C followed by refluxing in acetic acid medium. An inset shows a high resolution TEM micrograph of the as obtained product.

was calculated from the high temperature (200–300 K) data of the inverse susceptibility plot which shows the presence of only Mn(IV) at each stage, except the product obtained at 250 °C. At 250 °C, the magnetic moment per mole of Mn ion is 5.48 μ_B which corresponds to Mn(II). It seems that, at 250 °C, the small quantity of un-decomposed manganese oxalate containing Mn (II) is present and dominates the magnetic moment. All other products show that the magnetic moment corresponds to tetravalent manganese (Table 2). It may be noted that any admixture of lower-valent manganese would increase the magnetic moment. Hence, we conclude that the Mn(IV) oxidation state is maintained in the spinel phase. Interestingly, we have observed that the magnetic susceptibility value is highest (0.145 emu/g, at 10 K) for the nanorods with lower dimensions (obtained at 250 °C after reflux) (Fig. 12). Also, for the particles (obtained at 250 °C) of $Zn_{0.83}(Mn_{1.42}Zn_{0.34})O_4$ of lower dimensions (5–10 nm), the magnetic susceptibility is quite low (0.03 emu/g, at 10 K (Fig. 12). This is a rare example of transformation of nanospheres to nanorods involving tetravalent manganese ($Zn_{0.83}(Mn_{1.42}Zn_{0.34})O_4$). The slight deviation of the magnetic moments of the products (Table 2) from the theoretical value (3.88 μ_B) is possibly due to the disordering of Zn and Mn in the A and B sites of the spinel AB_2O_4 structure. This defect would create near-neighbour Mn^{4+}–O–Mn^{4+} linkages along the *c* axis which would affect the moment. The hexagonal $ZnMnO_3$ phase containing Mn(IV) (prepared at high pressure) shows an antiferromagnetic behavior with an effective magnetic moment of 3.9 μ_B and a Néel temperature of 18 K. The measured moment exactly matches the calculated moment for a Mn(IV) system. Blasco *et al.*[13] has investigated the magnetic moment for other compositions, $Zn_{1.7}Mn_{1.3}O_4$ and $Zn_{1.6}Mn_{1.4}O_4$ wherein the PXRD pattern was indexed on the basis of a cubic cell similar to the reported '$ZnMnO_3$'. The magnetic moment studies suggest that the above two compounds contain a mixture of Mn(III) and Mn(IV).[13] However, our magnetic and XPS studies unambiguously suggest the presence of only Mn(IV) in $Zn_{0.83}(Mn_{1.42}Zn_{0.34})O_4$. An inset of Fig. 11 shows the magnetic saturation down to 10 K. There are minor magnetic fluctuations at the same temperature for, previously reported, similar compositions ($Zn_{1.7}Mn_{1.3}O_4$).[13]

Experimental

Commercially available zinc nitrate hexahydrate (Merck, 99%), manganese(II) acetate tetrahydrate, $Mn(CH_3COO)_2{\cdot}4H_2O$, (CDH, 99%) and ammonium oxalate, $(NH_4)_2C_2O_4{\cdot}H_2O$, (S.D. Finechemicals, 99%) were used in the synthesis. Mixed metal oxalates of zinc and manganese were synthesized by a co-precipitation method. To 20 ml of an aqueous solution of zinc nitrate (0.1 M), 20 ml of aqueous manganese acetate (0.1 M) solution was slowly added and the solution was stirred for 2 h after which 40 ml of ammonium oxalate (0.1 M) was slowly added and then stirred overnight. The oxalate precursor was isolated by centrifugation, washed with acetone and then dried in air. The precursor was then calcined at various temperatures (250 °C, 450 °C and 600 °C) in air, followed by refluxing in acetic

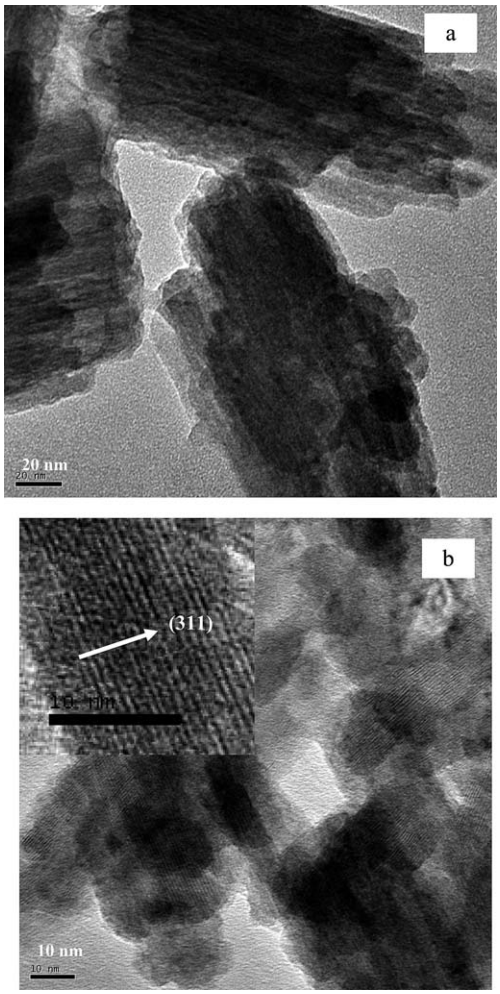

Fig. 9 $Zn_{0.83}(Mn_{1.42}Zn_{0.34})O_4$ nanorods synthesized by thermal decomposition at 450 °C followed by refluxing in acetic acid medium; (a) TEM and (b) HRTEM.

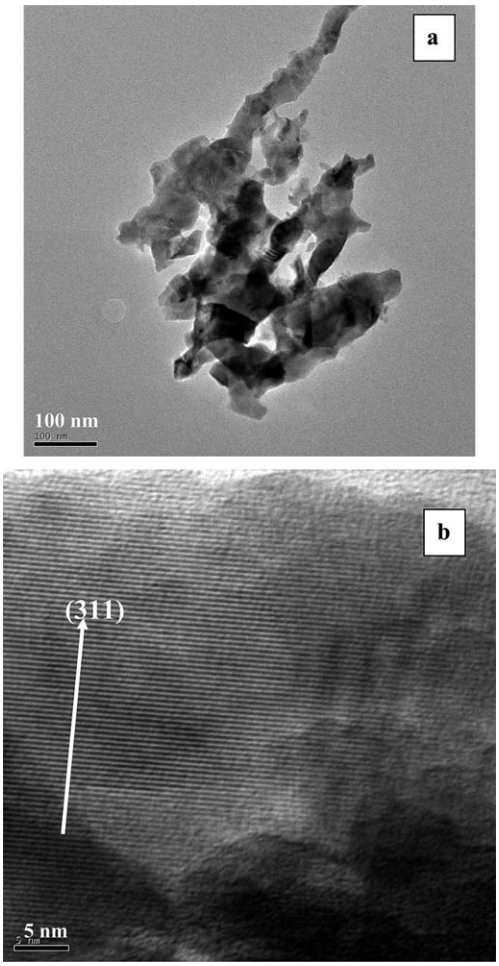

Fig. 10 $Zn_{0.83}(Mn_{1.42}Zn_{0.34})O_4$ nanorods synthesized by thermal decomposition at 600 °C followed by refluxing in acetic acid medium; (a) TEM and (b) HRTEM.

acid (0.1 M) medium at 120 °C for 6 h, yields the pure Zn–Mn–O spinel.

Powder X-ray diffraction (PXRD) studies were carried out on a Bruker D8 Advance diffractometer using Ni filtered Cu–Kα radiation with a step size of 0.02° and a step time of 1 s. Raw data were subjected to background correction and Kα_2 lines were removed. PXRD data for Rietveld refinement was collected using a step size of 0.02° and a step time of 8 s per step were used. Structural refinement was carried out using the TOPAS software[21] in the space group $Fd\bar{3}m$. The background was modeled by a shifted Chebyschev polynomial and the peak profile was simulated with a pseudo-Voigt function. The refinement involved the cell parameter, scaling factor, positional parameters, the isotropic thermal parameters for all atoms and the site occupancy factors. EDX data of the sample was obtained using a scanning electron microscope (Carl Zesis EVO 50 WDS electron microscope). The X-ray photoemission spectrum (XPS) was recorded in a Perkin–Elmer instrument, using Al–Kα radiation at 2×10^{-9} Torr base *vacuum*. Elemental analysis for Zn and Mn were performed using atomic absorption studies (atomic absorption spectrophotometer, analyst 100 Perkin–Elmer). TEM studies were carried out using a Tecnai G^2 20 electron microscope operated at 200 kV. TEM specimens were prepared on Cu grids by dispersing the oxide and oxalates in ethanol. Temperature and field dependent magnetization measurements were carried out by using a quantum design physical properties measurement system. The magnetization was measured at temperatures ranging from 3 to 300 K, in an applied field of 0.1 Tesla.

Table 2 Details of the magnetic studies of the zinc manganese oxide

Details	Magnetic study (antiferromagnetic)
1. At 250 °C, nanoparticles 5–10 nm)	Magnetic moment = 5.48 μ_B/Mn
2. 250 °C refluxed sample, nanorod (aspect ratio = 6)	Magnetic moment = 3.16 μ_B/Mn
3. At 450 °C, nanoparticles (10–20 nm)	Magnetic moment = 3.77 μ_B/Mn
4. 450 °C reflux sample, nanorods (aspect ratio = 10)	Magnetic moment = 3.60 μ_B/Mn
5. 600 °C reflux sample, nanorods (aspect ratio = 6–10)	Magnetic moment = 3.73 μ_B/Mn

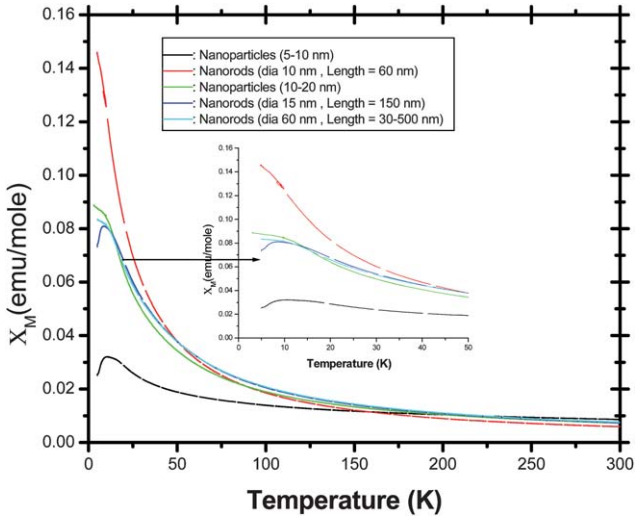

Fig. 11 Plot of magnetic susceptibility with temperature of $Zn_{0.83}(Mn_{1.42}Zn_{0.34})O_4$ obtained using co-precipitation route under different conditions (an inset show the X_M *vs.* T in lower temperature region).

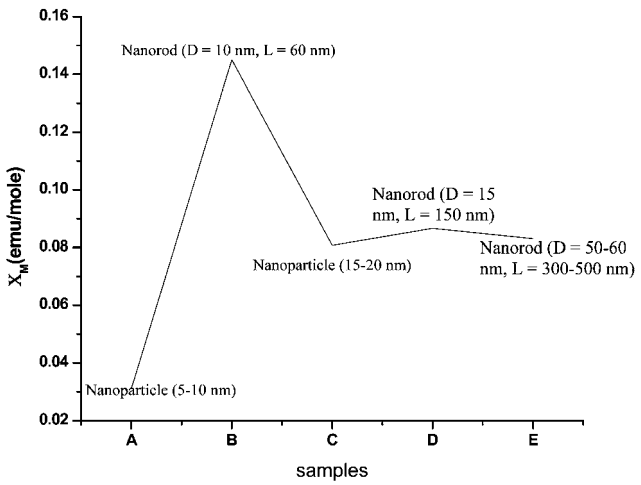

Fig. 12 Plot of magnetic susceptibility under different conditions at 60 K (**sample**: A: 250 °C, nanoparticle (5–10 nm); B: 250 °C, reflux (nanorod, diameter 10 nm, length = 60 nm); C: 450 °C (nanoparticles, 15–20 nm); D: 450 °C, reflux (nanorod, diameter = 15 nm, length = 150 nm); E: 600 °C, reflux (nanorod, diameter = 50–60 nm, length = 300–500 nm).

Conclusions

Nanorods and nanoparticles of $Zn_{0.83}(Mn_{1.42}Zn_{0.34})O_4$ containing only Mn(IV) have been successfully synthesized at low temperature (250 °C) and ambient pressure. Our methodology opens a new route for stabilizing higher oxidation states of manganese in complex zinc–manganese oxides. Nanoparticles and nanorods of variable dimensions have been synthesized at low temperature *via* a precursor mediated route. Our study developed a new single step process to transform nanospheres in to nanorods at low temperature. The phase is antiferromagnetic and the magnetic moment suggests the presence of only Mn(IV) which is also confirmed by XPS studies. The nanorods of smaller aspect ratio show higher magnetic moments/susceptibility compared to the rods of higher dimensions and also from nanosphere of any dimension.

Acknowledgements

AKG thanks the Nanomission, Department of Science & Technology, Govt. of India for the grant of the HRTEM and CSIR, Govt. of India for financial support. Menaka thanks UGC, Govt. of India for a fellowship. SEL acknowledges partial support from NSF grants DMR 0908779 and MRSEC DMR 0520471.

References

1 B. L. Chamberland, A. W. Sleight and J. F. Weiher, *J. Solid State Chem.*, 1970, **1**, 512–514.
2 V. G. Kumar and K. B. Kim, *Ultrason. Sonochem.*, 2006, **13**, 549–556.
3 Z. Li., Y. Ding, Y. Xiong and Y. Xie, *Cryst. Growth Des.*, 2005, **5**, 1953–1958.
4 X. Shen, Y. Ding, J. Liu, K. Lubernds, R. P. Zerger, M. Polverejan, Y. C. Son, M. Aindow and S. L. Suib, *Chem. Mater.*, 2006, **16**, 5327–5335.
5 S. G. Fritsch, C. Chanel, J. Sarrias, S. Bayonnea, A. Rousseta, X. Alcobe and M. L. M. Sarrio, *Solid State Ionics*, 2000, **128**, 233–242.
6 M. Peiteado, A. C. Caballero and D. Makovec, *J. Solid State Chem.*, 2007, **180**, 2459–2464.
7 Menaka, M. Qamar, S. E. Lofland, K. V. Ramanujachary and A. K. Ganguli, *Bull. Mater. Sci.*, 2009, **32**, 231–237.
8 Y. Bessekhaud, D. Robert and J. V. Weber, *Catal. Today*, 2005, **101**, 315–321.
9 S. Kolesnik, B. Dabrosky and J. Mais, *J. Supercond.*, 2002, **15**, 251–255.
10 S. Thota, T. Dutta and J. Kumar, *J. Phys.: Condens. Matter*, 2006, **18**, 2473–2486.
11 C. J. Cong, L. Liao, Q. Y. Liu, J. C. Li and K. L. Zhang, *Nanotechnology*, 2006, **1**, 1520–1526.
12 M. Peiteado, A. C. Caballero and D. Makovec, *J. Eur. Ceram. Soc.*, 2007, **27**, 3915–3918.
13 J. Blasco and J. Garcia, *J. Solid State Chem.*, 2006, **179**, 2199–2205.
14 S. L. Samal, W. Green, S. E. Lofland, K. V. Ramanujachary, D. Das and A. K. Ganguli, *J. Solid State Chem.*, 2008, **181**, 61–66.
15 M. K. El-Aiashy, H. S. Mazhar and S. M. Kamal, *Mater. Lett.*, 1995, **24**, 97–101.
16 F. C. M. Driessens and G. D. Rieck, *J. Inorg. Nucl. Chem.*, 1966, **28**, 1593–1600.
17 M. Peiteado, S. Sturm, A. C. Caballero and D. Macovec, *Acta Mater.*, 2008, **56**, 4028–4035.
18 L. V. Saraf, P. Nachimuthu, M. H. Engelhard and D. R. Baer, *J. Sol-Gel Sci. Technol.*, 2010, **53**, 141–147.
19 J. H. Li, D. Z. Shen, J. Y. Zhang, D. X. Zhao, B. S. Li, Y. M. Lu, Y. C. Liu and X. W. Fan, *J. Magn. Magn. Mater.*, 2006, **302**, 118–121.
20 H. Toussaint, *Rev. Chim. Miner.*, 1964, **1**, 141–95.
21 *Bruker AXS GmbH. Topas V4.2: General Profile and Structure Analysis Software for Powder Diffraction Data* ed; Bruker AXS GmbH, Karlsruhe, 2009.
22 B. Novosel, B. Tezak, Z. C. Elijas, A. Haraminiii, V. Jakopovic, B. Ryznar, M. Stiglit and M. Vidas, *Colloid Polym. Sci.*, 1976, **254**, 412–416.
23 T. Ahmad, S. Vaidya, N. Sarkar, S. Ghosh and A. K. Ganguli, *Nanotechnology*, 2005, **17**, 1236–1240.
24 T. Ahmad, K. V. Ramanujachary, S. E. lofland and A. K. Ganguli, *J. Mater. Chem.*, 2004, **14**, 3406–3410.
25 X. D. Zhang, Z. S. Wu, J. Zang, D. Li and Z. D. Zhang, *J. Phys. Chem. Solids*, 2007, **68**, 1583–1590.
26 M. M. Thackeray and A. D. Kock, *Mater. Res. Bull.*, 1993, **28**, 1041–1049.
27 M. Gaudon, N. Paihe, A. Wattiaux and A. Demourgues, *Mater. Res. Bull.*, 2009, **44**, 479–484.
28 J. T. Sampanthar, J. Dou, G. G. Joo, E. Widjaja and L. Q. H. Eunice, *Nanotechnology*, 2007, **18**, 025601–025609.
29 N. S. Bell and D. R. Tallant, *J. Sol-Gel Sci. Technol.*, 2009, **51**, 158–168.
30 T. I. Tsuruoka, S. Furukawa, Y. Takashima, K. Yoshida, S. Isoda and S. Kitagawa, *Angew. Chem., Int. Ed.*, 2009, **48**, 4739–4743.
31 F. Cheng, J. Zhao, W. Song, C. Li, H. Ma, J. Chen and P. Shen, *Inorg. Chem.*, 2006, **45**, 2038–2044.
32 R. Ranjan, S. Vaidya, P. Thaplyal, M. Qamar, J. Ahmed and A. K. Ganguli, *Langmuir*, 2009, **25**, 6469–6475.